Coatings **2014**, *4*, 701-714; doi:10.3390/coatings4040701

OPEN ACCESS

coatings

ISSN 2079-6412

www.mdpi.com/journal/coatings

Article

Morphology and Microstructure of NiCoCrAlYRe Coatings after Thermal Aging and Growth of an Al_2O_3-Rich Oxide Scale

Giovanni Di Girolamo [1,*], Alida Brentari [2] and Emanuele Serra [1]

[1] ENEA, Materials Technology Unit, Casaccia Research Center, Rome 00123, Italy; E-Mail: emanuele.serra@enea.it

[2] ENEA, Materials Technology Unit, Faenza Research Center, Faenza 48018, Italy; E-Mail: alida.brentari@enea.it

* Author to whom correspondence should be addressed; E-Mail: giovanni.digirolamo@enea.it.

External Editor: Ugo Bardi

Received: 14 July 2014; in revised form: 22 September 2014 / Accepted: 25 September 2014 / Published: 10 October 2014

Abstract: The surface of metal parts operating at high temperature in energy production and aerospace industry is typically exposed to thermal stresses and oxidation phenomena. To this aim, plasma spraying was employed to deposit NiCoCrAlYRe coatings on metal substrates. The effects of early-stage oxidation, at ~1100 °C, on their microstructure were investigated. The partial infiltration of oxygen through some open pores and microcracks embedded in coating microstructure locally assisted the formation of a stable Al_2O_3 scale at the splat boundary, while the diffusion of Cr and Ni and the following growth of Cr_2O_3, $Ni(Cr,Al)_2O_4$ and NiO were restricted to Al depleted isolated areas. At the same time, a continuous, dense and well adherent Al_2O_3 layer grew on the top-surface, and was somewhere supported by a thin mixed oxide scale mainly composed of Cr_2O_3 and spinels. Based on these results, the addition of Re to the NiCoCrAlY alloy is able to enhance the oxidation resistance.

Keywords: high temperature; coatings; atmospheric plasma spraying

---

1. Introduction

High-temperature coatings are commonly employed to protect the surface of metal components operating in energy production and aerospace industry, with the purpose to improve their resistance to oxidation and hot-corrosion phenomena, as well as to prolong their lifetime [1].

High-temperature coatings are also potential tools for increasing the efficiency of thermal engines. The application of ceramic thermal barrier coatings (TBCs) is particularly well-suited for this challenge, by reducing the heat flux and the temperature at the surface of the underlying component [2]. In this context, metal coatings can be successfully adopted to cover turbine components in order to improve their environmental resistance, without compromising their structural stability and mechanical strength [3–5]. Among them, the well-known MCrAlY (Me = Ni, Co or Ni/Co) coatings can be used as overlay coatings or in conjunction with an upper ceramic TBC [6,7].

Plasma spraying is a cost-effective technology to manufacture MCrAlY coatings. In this process, a gas plasma is employed as heat source to process the powder-based raw material. The powder particles are injected in the plasma jet by a carrier gas, and melted and accelerated toward the substrate, where they impact at high speed and quench, thus producing the build-up of a coating with unique microstructure.

The thermal exposure at elevated temperature promotes the formation of a thin oxide layer on the surface of MCrAlY coating during service [8,9]. However, the extended formation of secondary mixed oxides in conjunction with Al_2O_3 has been reported to be detrimental for coating durability. Indeed, their fast growth induces thermal stresses which can develop cracking and delamination, leading to the spallation of the upper TBC [10–13].

It has been reported that the addition of Re to MCrAlY based alloy is able to increase the related oxidation resistance as well as the mechanical properties. The improvement has been somewhat explained in terms of better high-temperature diffusion behavior of Al, that decreasing the extent of β-NiAl phase depletion within the coating and thus the oxidation rate and the scale spallation [14–16]. A significant enhancement in thermal fatigue resistance has been also noticed, since the addition of Re seemed to have a beneficial effect on the mechanism of crack formation and propagation [17]. Otherwise, other investigators reported that the addition of Re to the metallic alloy involved lower thermal expansion coefficient and higher hardness, but lower oxidation resistance [15].

The aim of this study was to develop atmospheric plasma sprayed NiCoCrAlYRe coatings with enhanced oxidation resistance by reducing the in-flight oxidation of the starting metal particles during processing and thus assisting the formation of an approximately dense and continuous Al_2O_3 rich scale during early stage isothermal exposure, in order to partially prevent the fast formation of extended mixed oxides and to enhance the oxidation resistance of these systems at high temperature. The microstructural and morphological changes were investigated by scanning electron microscopy (SEM) and energy dispersive spectroscopy (EDS).

2. Experimental Section

NiCoCrAlYRe coatings with thickness of about 150 μm were deposited on Ni-superlloy disks (ϕ = 25 mm, thickness = 4 mm) starting from a commercial powder feedstock (Sicoat 2453, Siemens

AG, Mulheim, Germany). An atmospheric plasma spraying (APS) system equipped with F4-MB plasma torch (Sulzer Metco, Wolhen, Switzerland) with 6 mm internal diameter nozzle was used for powder processing. The substrates were sand blasted with alumina abrasive powder (Metcolite F, Sulzer Metco, Westbury, NY, USA) to increase their surface roughness and to improve the mechanical adhesion between coating and substrate. The grain size of the abrasive particles was in the range between 350 and 1100 μm, as reported by the supplier. The blasting parameters employed were: air pressure = 0.45 MPa, gun-substrate distance = 10 mm, angle = 45° and spray time = 10 s. The specimens were then cleaned in ethanol, placed on a rotating sample holder and coated by successive torch passes. The processing parameters are reported in Table 1.

Table 1. Plasma spraying parameters used in this work.

Plasma spraying parameters	Value
Current [A]	600
Voltage [V]	67
Substrate tangential speed [mm/s]	1041
Gun velocity [mm/s]	4
Primary gas Ar flow rate [slpm *]	55.5
Secondary gas H_2 flow rate [slpm *]	9.5
Spraying distance [mm]	130
Carrier gas flow rate [slpm *]	2
Powder feed rate [g/min]	52
Distance torch-injector [mm]	6
Injector diameter [mm]	1.8

* slpm—standard liters per minute.

The surface roughness of substrates and coatings was measured using a 3D optical surface profilometer (New View 5000 system, Zygo Corporation, Middlefield, CT, USA). This white-light interferometer system allowed for study of the topography of the coating surface, which was previously metallized by Al thin film vacuum deposition (thickness = 40 nm), in order to allow reflection. The measurements were performed on areas of 0.7 × 0.5 μm^2. The interferogram of the coating surface was then processed and transformed to three-dimensional high-resolution surface image by frequency domain analysis. The arithmetic mean roughness value (R_a) was calculated as the average deviation of the surface profile from the mean line, defined by Equation (1):

$$R_a = \frac{\int_{x=0}^{x=L} |y(x)| \, dx}{L} \quad (1)$$

where y is the deviation of the surface profile from the centerline. The measured substrate roughness was found to be 6.9 ± 1.1 μm. In turn, the surface roughness R_a of the as-sprayed coatings was found to be 13.5 ± 0.4 μm. After plasma spray processing, the surface roughness doubled, depending on the size of the powder particles as well as on their momentum and flattening upon impact on the substrate surface.

After deposition the coated samples were heated at 5 °C/min, held at the maximum temperature of 1110 °C for 48 h and then cooled inside the furnace at 5 °C/min.

As-sprayed and aged samples were then cut by low-speed diamond saw and their cross sections were mounted in vacuum in two-part polymer, polished with diamond suspensions and finished to 0.25 μm. The morphology and the microstructure of as-sprayed and oxidized coating cross sections were analyzed by scanning electron microscope (SEM-Field Emission Gun, Leo Gemini mod. 1530, Carl Zeiss, Oberkochen, Germany) equipped with energy dispersive spectroscopy (EDS). EDS analysis was used to measure the composition of powder and coatings as well as to map the distribution of the constituents.

3. Results and Discussion

As shown in the SEM picture reported in Figure 1, the powder feedstock is composed of spherical particle agglomerates. The inset in the left corner of the same micrograph shows the detailed surface morphology of an agglomerate, characterized by grains with size lower and higher than 1 μm and with spherical, quasi-spherical and elongated shape. Some dendritic structures can be also observed. The grey contrast could be associated to fluctuations in Al content. The particle size distribution measured by SEM observations was in the range between 45 and 65 μm, while the average particle size was 54 ± 5 μm.

Figure 1. SEM spherical morphology of NiCoCrAlYRe particle agglomerates. Grains with submicrometer size can be observed on the surface.

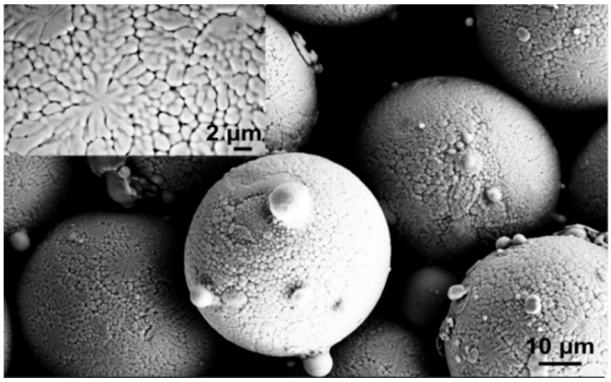

In turn Figure 2 shows the EDS map of powder particles, suggesting the presence of significant amount of Re and Y. The measured chemical composition (wt%) of the powder feedstock can be summarized as 52Ni 10Co 24Cr 10Al 1Y 3Re.

Figure 3a,b shows the cross sectional microstructure of plasma sprayed NiCoCrAlYRe coating at different magnification. The coating exhibits a lamellar microstructure composed of overlapped splats, originated by deformation and quenching of molten droplets at the substrate surface during deposition process. Some pores and splat boundaries can be observed. The former are related to filling defects produced by gas entrapped in the molten droplets during coating build-up, whereas the splat boundaries derived from weak bonding between the overlapped splats, depending on the temperature distribution along the same ones during cooling to room temperature.

A large and approximately uniform distribution of dark grey β-NiAl precipitates can be observed within the light-grey γ matrix, as detectable in Figure 3b. At splat boundary very restricted Al depletion and coalescence of β precipitates are also noticed. It is worth noting that these precipitates represent an Al reservoir for next selective oxidation.

Figure 2. Energy dispersive spectroscopy (EDS) map showing the composition of NiCoCrAlYRe powder particles.

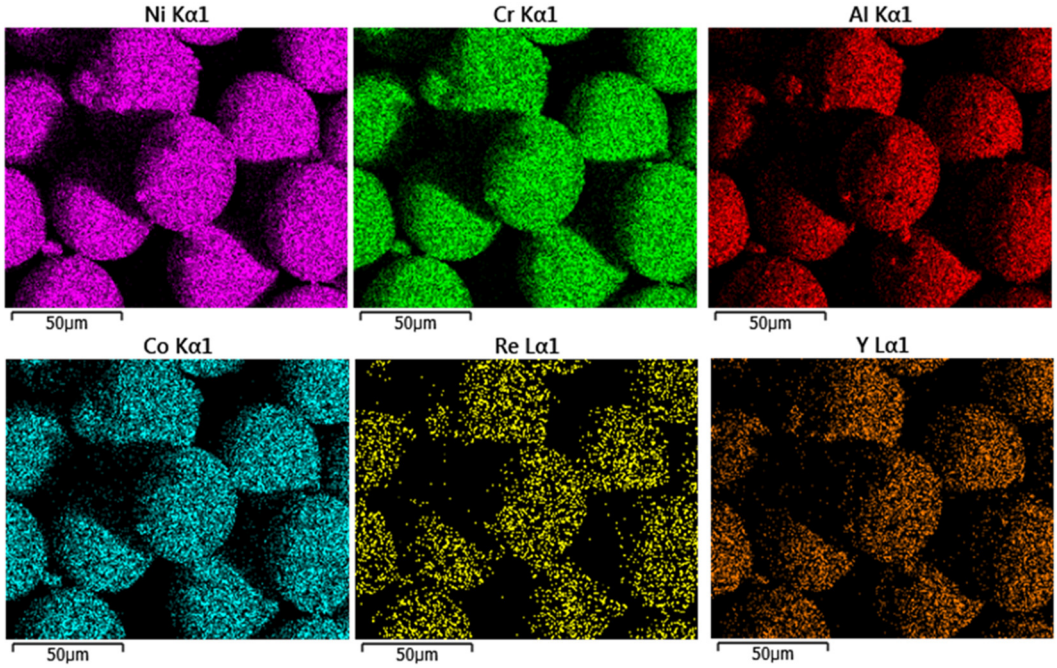

Figure 3. (**a**) Cross sectional SEM microstructure showing two-phase microstructure and typical defects of as-sprayed NiCoCrAlYRe coating; and (**b**) SEM micrograph showing coarser and finer β precipitates dispersed in the γ matrix.

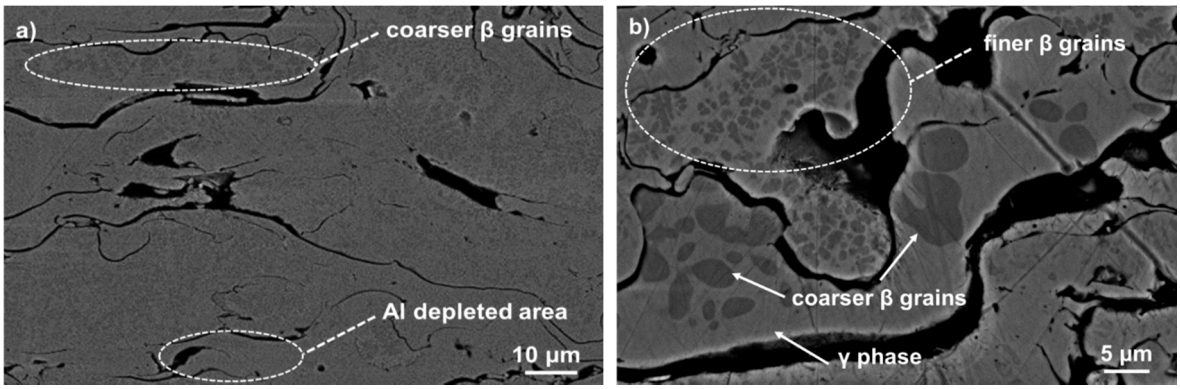

According to EDS analyses reported in Table 2, the areas rich with β precipitates contain about 18 wt% Al and are partially depleted in Cr and Re with respect to the γ phase, because of limited solubility of Re in the same β phase [18]. Indeed, the β phase contains 14 wt% Cr and 1 wt% Re, whereas the γ phase approximately contains 25 wt% Cr and 3 wt% Re.

It has been reported that high retention of β phase is usually obtained using HVOF (High Velocity Oxy Fuel) spraying, while APS coatings are mainly composed of γ phase because of higher oxidation rate experienced by the sprayed particles during processing [19]. However, in the present case the composition of the plasma gas mixture employed (total gas mixture flow = 65 slpm and Ar/H_2 ratio ~6) allowed for prevention of overheating and oxidation of the surface of the molten particles during spraying as well as the Al depletion. Indeed, the average content of Al did not decrease after spraying

(~10 wt%), as well as the average wt% Re, so that the composition of the as-sprayed coating was approximately equal to that of the starting powder particles.

Table 2. Chemical composition of as-sprayed NiCoCrAlYRe coating, matrix and β-rich areas.

Chemical element	As-sprayed coating (wt%)	γ Matrix (wt%)	β Phase rich area (wt%)
Ni	52.0 ± 0.2	51.2 ± 0.5	58.0 ± 1.4
Co	10.0 ± 0.1	10.0 ± 0.1	9.0 ± 0.3
Cr	23.9 ± 0.1	24.7 ± 1.1	14.0 ± 1.6
Al	10.5 ± 0.1	10.0 ± 1.0	18.0 ± 1.0
Y	0.7 ± 0.3	0.7 ± 0.3	–
Re	2.9 ± 0.3	3.3 ± 0.2	1.0 ± 0.6

Figure 4 shows a localized area in coating cross section which suffered internal oxidation during next high-temperature aging. The thermal exposure in air environment promoted the partial infiltration of oxygen through the open pores and microcracks located along coating thickness. Therefore, in some regions near the coating surface the penetration of oxygen promoted the Al diffusion from the β-NiAl phase and the following formation of a dark grey Al_2O_3 scale at splat boundary (the surface of metal particles), which typically surrounds the voids. In restricted areas the outward diffusion of Ni and Cr promoted further chemical reactions, leading to the growth of some mixed oxide scales on the Al_2O_3 surface. The growth of secondary oxide phases generally occurred in restricted areas where more pronounced Al depletion did not allow the formation of a stable and protective Al_2O_3 layer, whereas it was less significant in the areas characterized by growth of a continuous and well adherent Al_2O_3 layer.

Figure 4. A localized area characterized by internal oxidation within the cross sectional microstructure of NiCoCrAlYRe coating. After high-temperature aging dark grey alumina flakes grow at splat boundary and are somewhere supported by grey spinel-type porous oxides, whereas NiO appears in form of light grey precipitates embedded in the spinel phase.

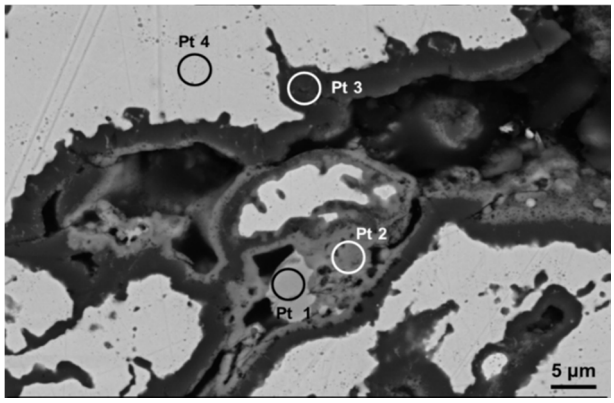

Figure 5 reports the EDS maps related to the area presented in Figure 4, demonstrating the formation of Al_2O_3 oxide scale at splat boundary as well as the formation of Cr_2O_3, $Ni(Cr,Al)_2O_4$ (medium grey phase) and NiO (light grey) at lesser extent in any localized areas with lower Al content [20]. It should be noted that the maps of Ni, Co, Cr and Re are well matched, thus suggesting the uniform distribution of these elements within the γ matrix. Figure 6 reports the EDS spectra related to different regions identified in coating microstructure, and denoted by circled areas in Figure 4. These spectra are

compatible with the presence of NiO, Cr_2O_3 + spinels, Al_2O_3 and γ matrix, respectively. In the Pt2 area a significant amount of Al (~8 wt%) was also found, this suggesting the presence of Al_2O_3 and $NiAl_2O_4$. In turn the presence of Cr suggested the formation of Cr_2O_3 and $NiCr_2O_4$. Otherwise, the wt% of Al in the depleted γ phase was found to be close to 4%, this suggesting a depletion of Al to form Al_2O_3 oxide at splat boundary. A slight decrease of Cr content has been noticed in the areas near the oxide layer, due to Cr diffusion and formation of its oxides. As clearly displayed in the elemental maps reported in Figure 5 as well as in the EDS analyses shown in Figure 6, the rhenium is uniformly distributed in the depleted γ matrix and its wt% was found to be 3.9% ± 0.5%, slightly higher than the related content observed in the matrix before high-temperature exposure (3.3 wt%), this suggesting Re diffusion from the β phase. Otherwise the presence of Re could not be observed in the oxidized areas. It is reasonable to suppose that Re was not directly affected by formation of its oxides, even if the formation of volatile Re_2O_7 could not be excluded. However, the addition of Re to the metal alloy played a positive role on the oxidation resistance, promoting better diffusion of Al and lower diffusion of other elements such as Ni and Cr, so that Al_2O_3 was the major oxidation product.

Figure 5. EDS maps showing the distribution of the elements in the oxidized region shown in Figure 4. Dark grey alumina scale grows at splat boundary and is somewhere supported by irregular grey mixed oxides.

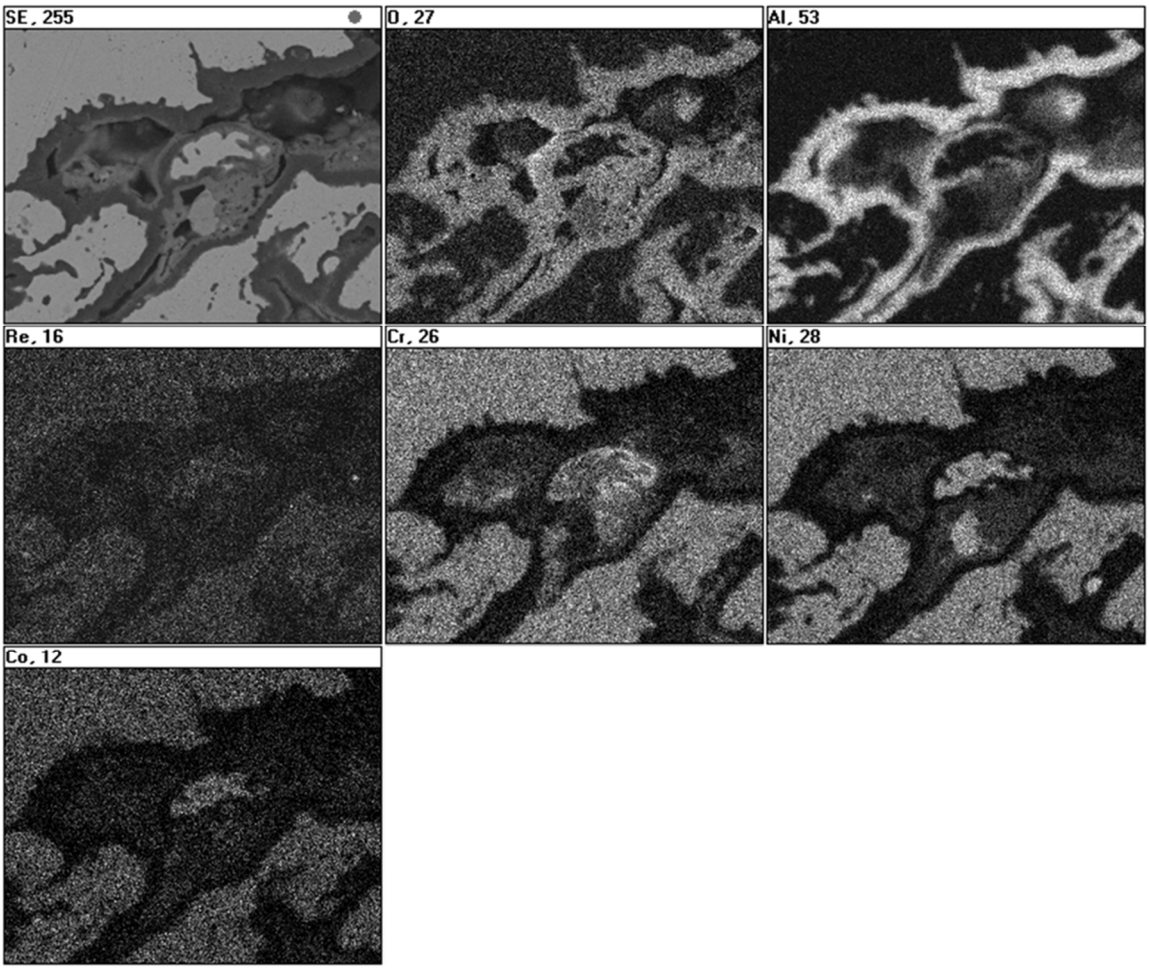

Figure 6. EDS spectra of different spot areas localized in coating microstructure, indicating the presence of (**a**) NiO; (**b**) Cr_2O_3 + spinels; (**c**) Al_2O_3; and (**d**) γ matrix.

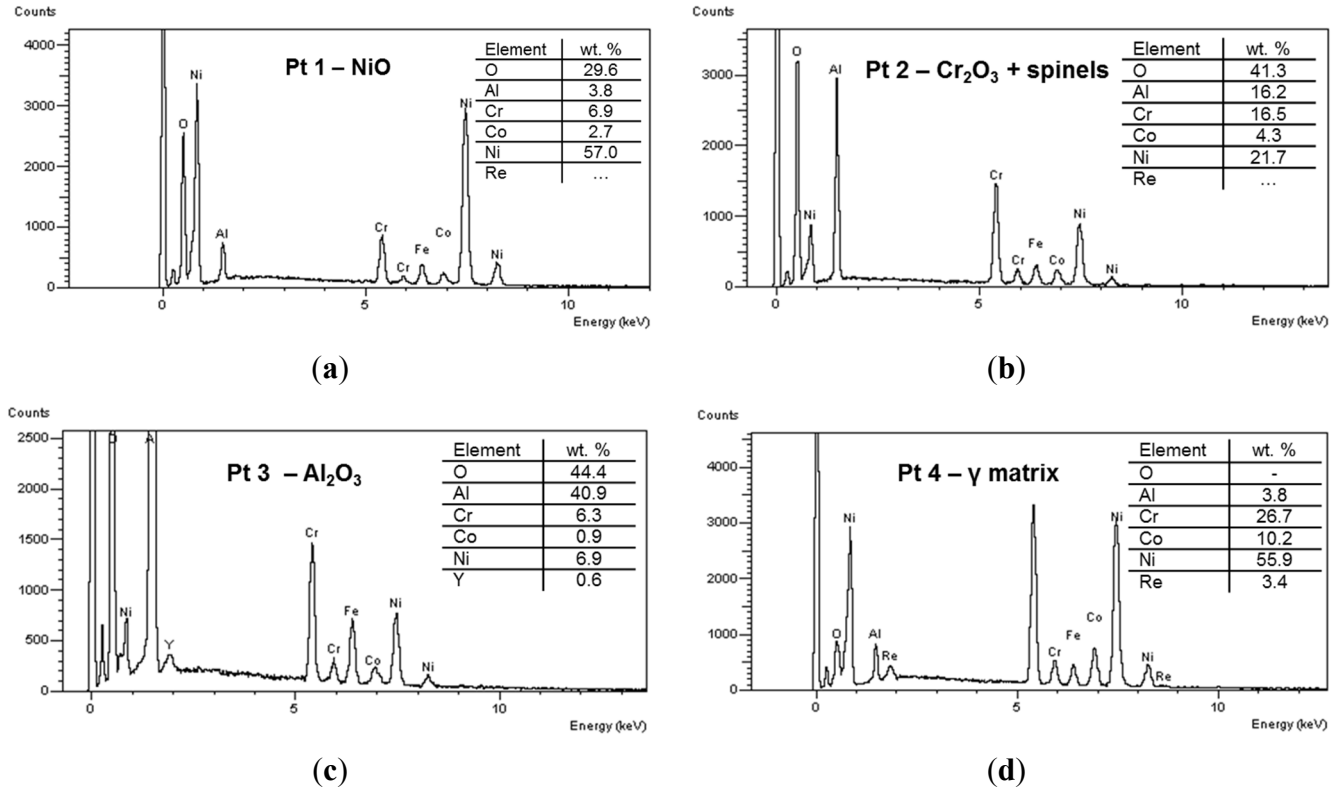

The most significant chemical reactions occurring during high-temperature exposure can be summarized as follows:

$$2Al + (3/2)O_3 \rightarrow Al_2O_3 \quad (2)$$

$$2Cr + (3/2)O_3 \rightarrow Cr_2O_3 \quad (3)$$

$$Ni + (1/2)O_2 \rightarrow NiO \quad (4)$$

$$NiO + Cr_2O_3 + Al_2O_3 \rightarrow Ni(Cr,Al)_2O_4 \quad (5)$$

As also reported by other authors, the spinel phases were formed because of reaction between Cr_2O_3 (or Al_2O_3) and NiO [20]. Based on the XRD results and phase composition study reported in a previous work as well as on the EDS analysis herein discussed it could be supposed that the spinel phase was mainly composed of $NiCr_2O_4$ [21].

It should be noted that it was very arduous to provide the exact composition of the various oxide scales detected, because their composition locally changed and the small volume considered for EDS measurements affected the quantitative results.

Figure 7 shows the cross-sectional microstructure near coating top-surface after early stage oxidation and suggests the formation of a double oxide scale, composed of an inner nearly continuous and dense alumina layer, followed by an upper and more brittle thin mixed oxide layer. As the oxidation time increased the formation of the Al_2O_3 scale on the coating surface occurred according to Equation (2). Al_2O_3 was the most thermodynamically stable oxide, so that Al_2O_3 mainly tended to grow after a

continuous TGO was developed. However, when Al was depleted to a certain extent near the coating top-surface Ni and Cr partially infiltrated through some cracks at nano scale across the growing Al_2O_3 layer, thus forming their oxides (NiO and Cr_2O_3) as well as spinels, via solid state reaction with pre-existing Al_2O_3 and C_2O_3 according to Equation (5). It is reasonable to suppose that the effect of the outward diffusion of Ni and Cr through the growing alumina layer was predominant with respect to that produced by inward oxygen infiltration, so that the mixed layer grew on the same Al_2O_3 layer. In addition, NiO and Cr_2O_3 could be formed at lesser extent in conjunction to Al_2O_3 during the first stage of thermal aging and then could react with the same Al_2O_3 to form spinels on the external surface.

Figure 7. Cross sectional SEM microstructure of oxidized NiCoCrAlYRe coating showing the formation of a double oxide scale on the top-surface, composed of an inner continuous Al_2O_3 scale supported by an upper mixed oxide layer.

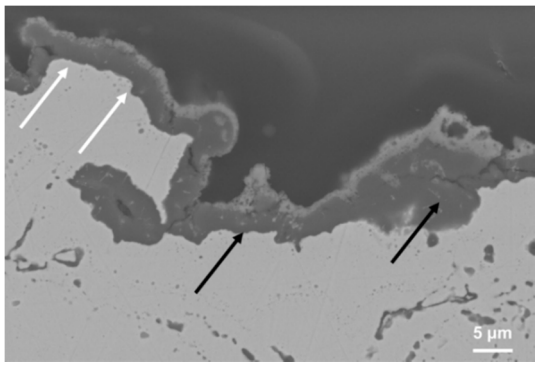

For this purpose the presence of the first stable alumina layer allowed for reduction of further oxygen infiltration, partially preventing the effect of internal oxidation, while the presence of the upper layer can represent a disadvantage, because some surface protrusions, derived from its fast and heterogeneous growth, and the thermal stresses herein originated can cause microcracking and delamination. However, if the coating had preserved a sufficient Al activity to allow the rehealing of the protective Al_2O_3 scale, the spallation of the outer mixed oxide layer does not represent a critical factor during the first hours of operation.

Otherwise, the same effect should be carefully taken in account when a ceramic TBC is applied on the NiCoCrAlYRe coating, because the thermal stresses generated at the interface and the horizontal microcraking can reduce the adhesion and thus promote unexpected TBC spallation during long-term service [22]. It is worth noting that the presence of a rough surface rich of asperities can partially impede the formation of a stable and continuous Al_2O_3 layer, allowing the fast formation of mixed oxide scale with embedded pores and microcracks. Indeed, as shown in Figure 7 the convex surface areas along the top-surface are characterized by the growth of a thin Al_2O_3 scale with an outer very thin spinel-type oxide scale (see the white arrows in the picture), while in the concave surface areas a thicker double oxide scale grew quickly, producing some surface protrusions, tensile stresses and microcracking (see the black arrows in the picture). High surface roughness increases the specific surface area for oxidation and also reduces the adhesion of the oxide scale during long-term service, as previously investigated [23]. The formation of mixed oxides has been also found in MCrAlY coatings deposited under vacuum atmosphere or by HVOF spraying and aged at 1000–1100 °C [24–26] and cannot be totally prevented, so that it is an important key issue to reduce their growth and to have a well adherent and dense oxide scale

mostly composed of Al_2O_3 with low oxygen diffusivity, and able to reduce permeation of Ni and Cr as well as further oxygen infiltration. For this purpose the NiCoCrAlYRe particles have been herein processed to fabricate coatings with the above mentioned two phase structure, by reducing in-flight oxidation at their external surface and thus preventing Al depletion. The resulting high retention of β precipitates in the matrix allows for controlling at some extent the oxide scale formation during next high-temperature exposure. High process gas flow (Ar + H_2 = 65 slpm) and Ar/H_2 ratio (~6) were employed for melting and transport of melted particles in the plasma jet, in order to prevent metal surface oxidation during processing in air environment.

The simultaneous presence of different oxides can be also appreciated from the analysis of Figures 8 and 9. According to the EDS maps the presence of Al_2O_3 can be noticed as well as the formation of light grey structures particularly enriched in Cr. Figure 10a shows some metallic grains with size close to hundreds of nanometers and located below the TGO layer. The surface oxide layer was mechanically removed to observe their morphology and to calculate their composition, which was close to that of the depleted γ phase (see, for example, the graph 4 reported in Figure 6). Columnar and equiaxed grains of Al_2O_3 can be observed in the center of Figure 10b. In turn, Figure 10c shows some different structures larger than 1 μm and composed of a mixture of $NiCr_2O_4$ and NiO (see also the elemental map in Figure 8).

Figure 8. EDS maps of a localized region on the oxidized coating top-surface. The formation of mixed oxide scales composed of Ni, Al and Cr can be appreciated.

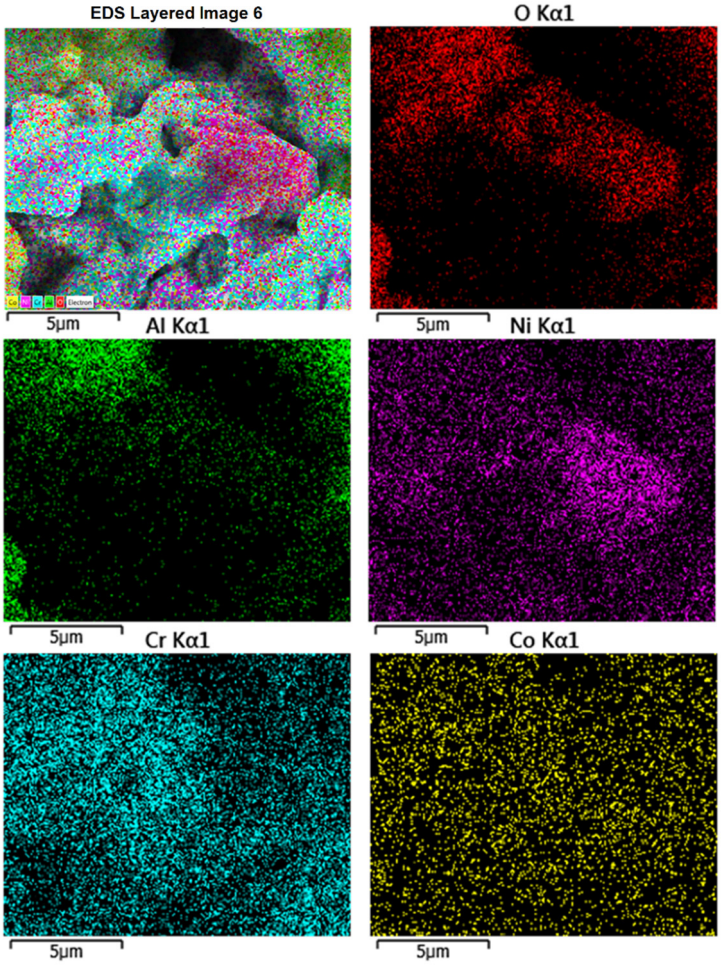

Figure 9. A localized area on oxidized coating top-surface characterized by the presence of mixed oxides grown on the surface of Al_2O_3 grains. NiO and spinels show polygonal and equiaxed shape, respectively.

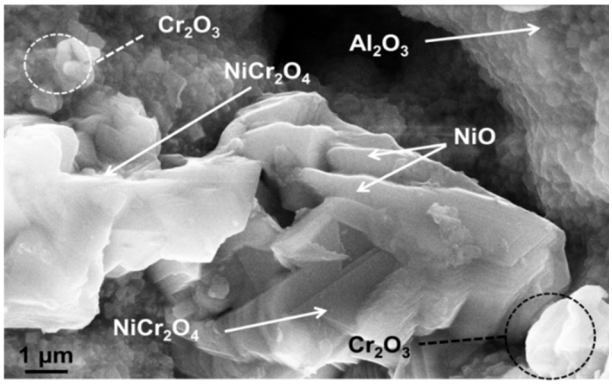

Figure 10. SEM morphology of (**a**) metal grains after removal of the oxide layer; (**b**) Al_2O_3 grains grown at the boundary of metal particles; and (**c**) mixed oxide scales with polygonal (NiO) and equiaxed shape (spinels).

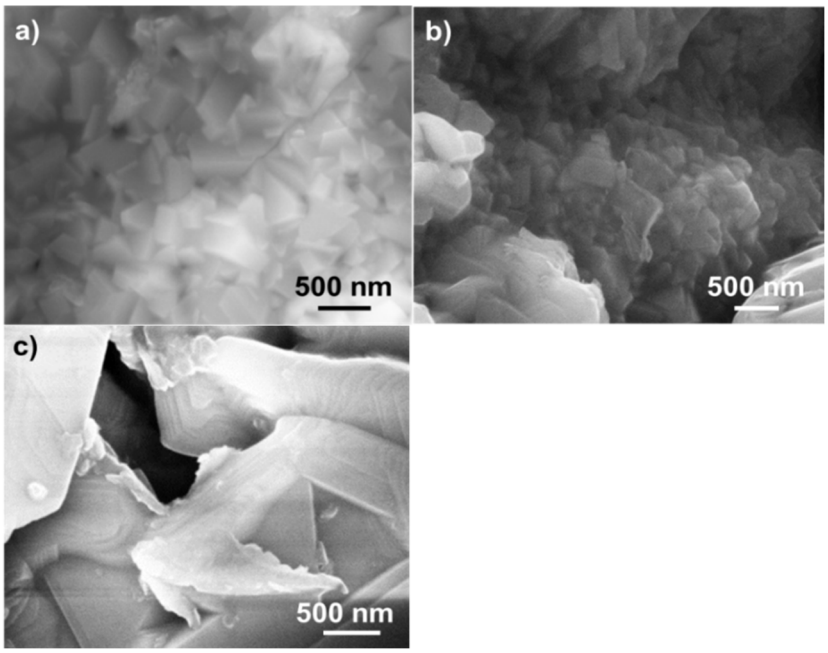

Generally, the NiO scale exhibited granular or polygonal/elongated shape, while spinels and Cr_2O_3 were present in form of equiaxed grains. The presence of these mixed oxide structures was appreciated in restricted and small areas where Al exhibited a reduced activity and its concentration was not enough to promote the selective formation of the preferable Al_2O_3 scale [20]. Based on the results discussed herein, the addition of Re to the NiCoCrAlY alloy allows for prevention of Al depletion during processing, thus involving high retention of β phase in the as-sprayed coating. Therefore, it plays a beneficial role on the related oxidation resistance at high temperature by improving Al diffusion and reducing the outward diffusion of elements like Cr and Ni. In other words, the presence of Re in the microstructure is useful to promote the formation of a protective, well adherent, dense and quasi continuous Al_2O_3 layer at metal surface, so that the formation of mixed oxide scales is reduced at lower

extent as well as the internal oxidation occurring at splat boundaries. Therefore, the β phase depletion and the oxidation rate of MCrAlYRe coatings are lower with respect to the conventional MCrAlY ones [6]. The addition of Re influences the morphology and the amount of the phases into the coating.

The studies concerning the composition and the microstructure of NiCoCrAlYRe overlay coatings can potentially affect their temperature capability and durability under different scenarios and be addressed to applications in power plants and aircraft engines. For this purpose, the systems used for propulsion typically experience multiple thermal cycles, whereas the power systems largely operate in isothermal mode with a few cycles. In addition the oxidation rate and the TGO growth become more critical when a ceramic TBC is applied on the metal coating, because the formation of the TGO at the interface between bond coat and top coat strongly affects the adhesion and the failure of the same TBC. Apart from the different operating conditions (temperature, cycling, presence of corrosive media and coating architecture) the oxidation mechanism of the metal coatings—including type, thickness, morphology and adhesive strength of the TGO—should be controlled at some extent to enhance coating performance.

4. Conclusions

The relative dense microstructure of NiCoCrAlYRe coatings, deposited by atmospheric plasma spraying, was characterized by high retention of well dispersed β-NiAl precipitates in the γ matrix. β grain coalescence and no Al depletion were observed after processing. Then high-temperature aging produced some effects of oxidation and oxide scale formation. In localized areas the presence of open pores and splat boundaries assisted partial oxygen infiltration through the coating thickness, promoting the formation of a continuous and dense Al_2O_3 scale at splat boundary. The diffusion of Cr and Ni assisted minor formation of Cr_2O_3, $Ni(Cr,Al)_2O_4$ and NiO on the surface of the same Al_2O_3 scale. At the same time, the oxidation of coating top-surface promoted the growth of an oxide scale, mainly composed of an inner continuous and well adherent Al_2O_3 layer, somewhere followed by an upper mixed oxide scale. The alumina layer was composed of grains with size of hundreds of nanometers, while the above mentioned mixed oxides tended to form complex micronsized/nanosized structures with polygonal and equiaxed shape. Based on these results, the addition of Re to the NiCoCrAlY alloy allowed for prevention of Al depletion during processing, thus involving high retention of β phase in the as-sprayed state. Moreover, it was able to improve Al diffusion and to partially prevent the outward diffusion of elements as Cr and Ni during high-temperature exposure. This was beneficial for promoting the growth of a protective, well adherent, dense and quasi continuous Al_2O_3 layer at the metal surface, so that the formation of mixed oxide scales was reduced at lower extent as well as the β phase depletion and the internal oxidation of the coating. For this purpose, further studies are needed to get a full understanding of the complex effect of Re addition on the oxidation resistance of NiCoCrAlYRe coatings.

Acknowledgments

The authors wish to thank C. Blasi for her valuable contribution during plasma spraying.

Authors Contribution

G.D. designed the experiments and analyzed the data; A.B. and E.S. contributed analysis tools and performed microstructural analyses.

Conflicts of Interest

The authors declare no conflict of interest.

References

1. Davis, J.R. *Handbook of Thermal Spray Technology*; ASM International: Materials Park, OH, USA, 2004.
2. Clarke, D.R.; Levi, C.G. Materials design for the next generation thermal barrier coatings. *Annu. Rev. Mater. Res*. **2003**, *33*, 383–417.
3. Taylor, M.P. An oxidation study of an MCrAlY overlay coating. *Mater. High Temp*. **2005**, *22*, 433–436.
4. Pollock, T.M.; Lipkin, D.M.; Hemker, K.J. Multifunctional coating interlayers for thermal-barrier systems. *MRS Bull*. **2012**, *7*, 923–931.
5. Di Girolamo, G.; Pagnotta, L. Thermally sprayed coating for high-temperature applications. *Rec. Pat. Mater. Sci*. **2011**, *4*, 173–190.
6. Di Girolamo, G.; Alfano, M.; Pagnotta, L.; Taurino, A.; Zekonyte, J.; Wood, R.J.K. On the early stage isothermal oxidation of APS CoNiCrAlY coatings. *J. Mater. Eng. Perf*. **2012**, *21*, 1989–1997.
7. Haynes, J.A.; Ferber, M.K.; Porter, W.D. Thermal cycling behavior of plasma-sprayed thermal barrier coatings with various MCrAIX bond coats. *J. Therm. Spray Technol*. **2000**, *9*, 38–48.
8. Daroonparvar, M.R.; Hussain, M.S.; Mat Yajid, M.A. The role of formation of continues thermally grown oxide layer on the nanostructured NiCrAlY bond coat during thermal exposure in air. *Appl. Surf. Sci*. **2012**, *261*, 287–297.
9. Mercer, C.; Hovis, D.; Heuer, A.; Tomimatsu, T.; Kagawa, Y.; Evans, A.G. Influence of thermal cycle on surface evolution and oxide formation in a superalloy system with a NiCoCrAlY bond coat. *Surf. Coat. Technol*. **2008**, *202*, 4915–4921.
10. Ni, L.Y.; Liu, C.; Huang, H.; Zhou, C.G. Thermal cycling behavior of thermal barrier coatings with HVOF NiCrAlY bond coat. *J. Therm. Spray Technol*. **2011**, *20*, 1133–1138.
11. Chen, W.R.; Wu, X.; Marple, B.R.; Patnaik, P.C. The growth and influence of thermally grown oxide in a thermal barrier coating. *Surf. Coat. Technol*. **2006**, *201*, 1074–1079.
12. Evans, A.G.; Mumm, D.R.; Hutchinson, J.W.; Meier, G.H.; Petit, F.S. Mechanisms controlling the durability of thermal barrier coatings. *Prog. Mater. Sci*. **2001**, *46*, 505–553.
13. Rabiei, A.; Evans, A.G. Failure mechanisms associated with the thermally grown oxide in plasma-sprayed thermal barrier coatings. *Acta Mater*. **2000**, *48*, 3963–3976.
14. Czech, N.; Schmitz, F.; Stamm, W. Improvement of MCrAlY coatings by addition of rhenium. *Surf. Coat. Technol*. **1994**, *68–69*, 17–21.
15. Liang, J.J.; Wei, H.; Zhu, Y.L.; Sun, X.F.; Hu, Z.Q.; Dargush, M.S.; Yao, X.D. Influence of Re on the properties of a NiCoCrAlY coating alloy. *J. Mater. Sci. Technol*. **2011**, *27*, 408–414.

16. Beele, W.; Czech, N.; Quadakkers, W.J.; Stamm, W. Long term oxidation tests on a Re-containing MCrAlY coating. *Surf. Coat. Technol*. **1997**, *94–95*, 41–45.
17. Czech, N.; Schmitz, F.; Stamm, W. Microstructural analysis of the role of rhenium in advanced MCrAlY coatings. *Surf. Coat. Technol*. **1995**, *76–77*, 28–33.
18. Huang, W.; Chang, Y.A. A thermodynamic description of the Ni-Al-Cr-Re system. *Mater. Sci. Eng. A* **1999**, *259*, 110–119.
19. Di Ferdinando, M.; Fossati, A.; Lavacchi, A.; Bardi, U.; Borgioli, F.; Borri, C.; Giolli, C.; Scrivani, A. Isothermal oxidation resistance comparison between air plasma sprayed, vacuum plasma sprayed and high velocity oxygen fuel sprayed CoNiCrAlY bond coats. *Surf. Coat. Technol*. **2010**, *204*, 2499–2503.
20. Liang, G.Y.; Zhu, C.; Wu, X.Y.; Wu, Y. The formation model of Ni-Cr oxides on NiCoCrAlY-sprayed coating. *Appl. Surf. Sci*. **2001**, *257*, 6468–6473.
21. Di Girolamo, G.; Brentari, A.; Blasi, C.; Pilloni, L.; Serra, E. High-temperature oxidation and oxide scale formation in plasma sprayed CoNiCrAlYRe coatings. *Metall. Mater. Trans. A* **2014**, *45*, 5362–5370.
22. Wright, P.K.; Evans, A.G. Mechanisms governing the performance of thermal barrier coating. *Curr. Opin. Solid State Mater. Sci*. **1999**, *4*, 255–265.
23. Gil, A.; Shemet, V.; Vassen, R.; Subanovic, M.; Toscano, J.; Naumenko, D.; Singhiser, L.; Quadakkers, W.J. Effect of surface condition on the oxidation behavior of MCrAlY coatings. *Surf. Coat. Technol*. **2006**, *201*, 3824–3828.
24. Tang, F.; Ajdelsztajn, L.; Kim, G.E.; Provenzano, V.; Schoenung, J.M. Effects of surface oxidation during HVOF processing on the primary stage oxidation of a CoNiCrAlY coating. *Surf. Coat. Technol*. **2004**, *185*, 228–233.
25. Poza, P.; Grant, P.S. CoNiCrAlY coatings after heat treatment and isothermal oxidation. *Surf. Coat. Technol*. **2006**, *201*, 2887–2896.
26. Saeidi, S.; Voisey, K.T.; McCartney, D.G. The effect of heat treatment on the oxidation behavior of HVOF and VPS CoNiCrAlY coatings. *J. Therm. Spray Technol*. **2009**, *18*, 209–216.